Wall correction factor for sinking cylinders in fluids

Gerald H. Ristow
Fachbereich Physik, Philipps-Universität, Renthof 6, 35032 Marburg, Germany
(Received 29 February 1996; revised manuscript received 22 July 1996)

Using finite difference methods, we study numerically the dynamics of a single spherical object (cylinder) in a two-dimensional box filled with viscous fluid under the influence of gravity. The algorithm is validated using the analytic result of the terminal velocity U_∞ in the creeping flow limit. We focus on the dependence of U_∞ on the cylinder diameter D and the box size L. By extrapolating the numerically obtained terminal velocities to the Stokes' limit $L\to\infty$ $(D/L\to 0)$ for various cylinder diameters, we seek a universal relation $U_\infty(D/L)=U_\infty(0)f(D/L)$ in analogy to the three-dimensional result for spheres in the creeping flow limit. We will present $f(D/L)$ as power series in D/L, and discuss its validity. [S1063-651X(97)08903-4]

PACS number(s): 47.55.Kf, 47.11.+j, 02.70.Bf

I. INTRODUCTION

When dropped in a vacuum tube, all bodies will fall with the same velocity, and will be accelerated by the gravitational constant g until they hit the floor. This is no longer true when particles are dropped in a surrounding fluid (or gas). An additional viscous force acts on the particle, and leads in the equilibrium of forces to a constant sinking velocity, called *terminal velocity*. This velocity not only depends on the size of the particle and the viscosity of the fluid, but also on the container geometry. From the Navier-Stokes equations in the creeping flow limit one can derive an analytic expression for the terminal velocity for spheres moving in bounded and unbounded three-dimensional geometries [1]. The ratio of the sphere velocity in the bounded and unbounded case is called the *wall correction factor*. For two-dimensional systems, the creeping flow equations do not have a physical solution, but an implicit expression for the terminal velocity of a cylinder can be obtained by using Oseen's equations [1,2]. No analytic expression for the wall correction factor for cylinders is known.

While cylinders sink in viscous fluids, one finds flow separation, wake oscillation, and wake shedding with increasing Reynolds number which has been studied extensively. A literature review is given by Clift, Grace, and Weber [3]. Some recent numerical simulations concerning the two-dimensional flow around cylinders are (a) Fornberg [4], who studied the viscous flow past a circular cylinder and investigated the width and length of the wake region; (b) Feng, Hu, and Joseph [5], who looked at the sedimentation of circular and elliptical particles and studied their interactions with the fluid, the wall, and each other; and (c) Chen, Pritchard, and Tavener [6] who investigated the stability and bifurcation of steady flow past a circular cylinder by looking at the formation of steady vortex pairs. We will use extensive numerical simulations of the full Navier-Stokes equations to simulate the sinking of cylinders in two-dimensional, bounded geometries. The obtained terminal velocities agree perfectly well with the implicit expression for low Reynolds numbers when finite-size effects of the numerical algorithm are taken into account [7]. By using nine different system sizes we are able to give, as an approximation of the wall correction factor for cylinders, an expression up to second order in the ratio cylinder to system size. By doing this for nine different cylinder diameters, we seek a *universal* curve for the wall correction factor up to moderate cylinder to system ratios and discuss its validity.

The paper is organized in the following way: in Sec. II we write down the relevant equations and give the terminal velocity for spheres and cylinders in the creeping flow limit. In Sec. III, we briefly explain the numerical technique used and present a first approximation of the wall correction factor for cylinders in Sec. IV. We conclude this paper by giving an outlook to possible further applications.

II. PHYSICAL BACKGROUND

Since the velocities in our situation are well below the speed of sound, the fluid is treated as incompressible. The dynamics of the fluid are then given by the following Navier-Stokes equations written in dimensionless units:

$$\frac{\partial\vec{v}}{\partial t}+(\vec{v}\cdot\boldsymbol{\nabla})\vec{v}=-\boldsymbol{\nabla}p+\frac{1}{\mathrm{Re}}\nabla^2\vec{v}+\vec{f}, \tag{1}$$

where $\vec{v}$ stands for the fluid velocity and p for the pressure measured in a fixed laboratory system. A possible external volume force, e.g., gravity, is denoted by $\vec{f}$. The continuity equation simplifies to

$$\boldsymbol{\nabla}\cdot\vec{v}=0. \tag{2}$$

The only parameter that describes the physical situation is the dimensionless Reynolds number Re. Given a characteristic velocity U, a characteristic length L and the viscosity of the fluid $\nu:=\eta/\rho$, its definition is

$$\mathrm{Re}:=\frac{UL}{\nu}. \tag{3}$$

In our case U will be the terminal velocity of the particle and L its diameter.

When a sphere moves through a fluid, a viscous friction force acts on it. In an ideal three-dimensional system where the fluid is at rest at infinity, this viscous force can be di-

rectly calculated from Eqs. (1) in the creeping flow limit where one neglects the inertia term $(\vec{v}\cdot\nabla)\vec{v}$ (Re$\ll$1) and obtains [1,2,8]

$$F_v = 6\pi\eta v r. \tag{4}$$

Here r stands for the radius of the sphere and v for its velocity. When this sphere moves under the influence of gravity its velocity exponentially reaches a limiting value which can be calculated from the equilibrium of forces,

$$v_s = \frac{2}{9}\frac{\rho_s-\rho_f}{\eta} g r^2. \tag{5}$$

Here ρ_s denotes the density of the sphere and ρ_f the one of the fluid. When the sphere moves in bounded geometries, e.g., a long tube with radius R, a wall correction factor has to be added which can be written as a polynomial in r/R only. For large aspect ratios r to R, considering only the linear term is often sufficient, and one obtains

$$v_s' = v_s\left(1-\alpha\frac{r}{R}\right), \tag{6}$$

where $\alpha\approx 2.1-2.4$ [1,3,9].

In two dimensions, the creeping flow equations do not have a solution that vanishes at the cylinder boundaries and remains finite at infinity which is known as Stokes' paradox [1]. If one works with Oseen's equations, an implicit formula for the terminal velocity can be given [1,2] which can only be solved numerically, e.g., using MATHEMATICA or MAPLE,

$$\frac{v_c}{\ln\left(3.7\frac{\nu}{r v_c}\right)} = \frac{1}{4}\frac{\rho_c-\rho_f}{\eta} g r^2. \tag{7}$$

Another interesting situation arises when the moving particle approaches another particle or a solid wall. Due to the backflow of the fluid, additional repulsive forces come into play that diverge as the inverse of the separation distance [10]. For ideal smooth surfaces this would mean that the surfaces never touch each other. This behavior is visible in our simulations when a particle approaches the bottom wall. It decelerates due to the additional forces from the backflow of the fluid, but very fine grids are needed to obtain quantitative data. The results presented in this paper are merely concerned with the terminal velocity and its dependence on $D=2r$ and the system size L. The system is sketched in Fig. 1, and the height was chosen as $H=3L$ to assure that the value of the terminal velocity was not affected by the presence of the bottom wall.

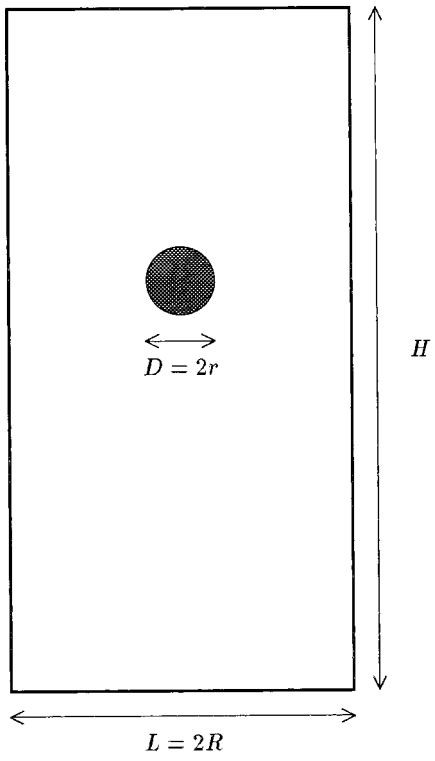

FIG. 1. Sketch of the physical system.

III. NUMERICAL IMPLEMENTATION

When Eqs. (1) are discretized in time first, the general form reads

$$\frac{\vec{v}^{n+1}-\vec{v}^{n}}{\Delta t} + \theta\left[(\vec{v}^{n+1}\cdot\nabla)\vec{v}^{n+1} - \frac{1}{\mathrm{Re}}\nabla^2\vec{v}^{n+1} - \vec{f}^{n+1}\right] + (1-\theta)\left[(\vec{v}^{n}\cdot\nabla)\vec{v}^{n} - \frac{1}{\mathrm{Re}}\nabla^2\vec{v}^{n} - \vec{f}^{n}\right] + \nabla p^{n+\tau} = 0, \tag{8}$$

where the parameter θ fulfills $0<\theta<1$. For $\theta=0$ we end up with an *explicit* scheme, and for $\theta=1$ we get a *fully implicit* scheme. The former has the advantage that the finite difference scheme can be written down more easily, but the restrictions on the maximal time step for numerical stability made it infeasible for our case [11,7]. A very efficient method results for $\theta=\frac{1}{2}$ called the *Crank-Nicolson scheme*, which we used to obtain the results presented in this paper. It is second order accurate in time as well, when the parameter τ is set to a value of $\frac{1}{2}$. The partial differential equations are solved by an iterative procedure which is based on applying the *artificial compressibility method* at each time step [11,12]. Since the scheme in Eq. (8) is linearly unconditionally stable for $\theta\geqslant\frac{1}{2}$, one can choose a maximal time step given by the physical situation, which in our case was a fraction of the grid size divided by the estimated terminal velocity. This allows us to obtain the terminal velocity of a sinking particle with much fewer time steps as compared to an explicit algorithm.

In order to avoid unphysical oscillations in the solutions we use a *staggered grid* [13] which is usually referred to as *marker-and-cell* (MAC) method [11]. Each grid point on which a particular velocity component is evaluated is shifted half a grid spacing along its Cartesian direction with respect to the corresponding pressure value. Another advantage of this grid is that no boundary values for the pressure are needed, which is often not available or hard to obtain experimentally. The pressure is only calculated at interior points. The generalization of the MAC grid to three spatial dimensions is straight forward.

Since we want to study the motion of particles in fluids, we have to account for the interactions between particles and fluid. For simplicity, we will only treat spherical particles in

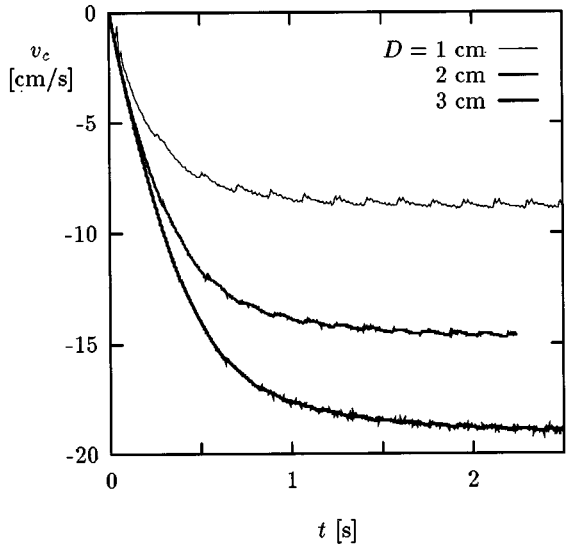

FIG. 2. Vertical velocity as a function of time for different cylinder diameters, $D=1$, 2, and 3 cm (top to bottom), respectively.

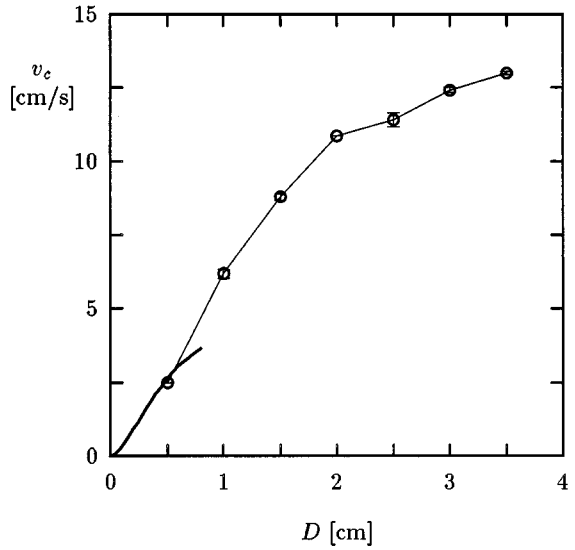

FIG. 3. Extrapolated terminal velocity for the limit $\Delta x \to 0$ as a function of cylinder diameter. The thick line in the lower left corner is the analytic solution using Oseen's equations.

two-dimensional boxes, but other shapes can be easily constructed. The grid spacings in different directions are all chosen as being equal $\Delta x \equiv \Delta y (\equiv \Delta z)$. They must be chosen significantly smaller than the particle in order for our approach to work. We used values of $D=(3-22)\times\Delta x$ for the results presented in this paper. The particle can be put at any arbitrary position in the fluid and all velocity grid points that are covered by the particle will be forced to have the particle's velocity at the next time step. This means that the particle introduces an additional, moving boundary to our computation. The force acting on the particle by the fluid is calculated by integration of the stress tensor σ over the particle's surface [10],

$$F_s = \int_{\text{surface}} \boldsymbol{\sigma} \cdot \vec{n} dA, \tag{9}$$

where $\vec{n}$ stands for the normal vector of a surface element pointing outwards and

$$\boldsymbol{\sigma} = -pI + \eta(\nabla \vec{v} + (\nabla \vec{v})^t). \tag{10}$$

Here a matrix notation is used, and I stands for the unity matrix. The stress tensor is evaluated along the Cartesian coordinate lines from interior to exterior points along the surface.

IV. WALL CORRECTION FACTOR

At time $t=0$, we place a cylinder at rest in our two-dimensional system sketched in Fig. 1. The force acting on the cylinder is calculated via integration of the stress tensor over its surface. For small times the sinking velocity is given by $v_s(t) \approx -gt$, since the viscous forces are still negligible. With increasing velocity the viscous forces become larger, and finally an equilibrium of forces leads to a constant sinking velocity which depends on the diameter D, the system dimension L, and the viscosity of the fluid η. This is shown in Fig. 2, where the sinking velocity as function of time is presented for three different cylinder diameters and a box dimension of 25×75 cm. The approach of the terminal velocity is clearly visible. The rather regular fluctuations for the smallest particle, $D=1$ cm, stem from the fact that the particle covered at most five grid points compared to already 25 for $D=2$ cm. Since it falls nearly vertically with a constant velocity, the variations in the number of grid points covered by the particle and used in the force calculation are relatively large, and they lead to visible regular oscillations. For larger particles, these regular patterns disappear and the remaining fluctuations come from the fluid motion.

In Ref. [7], we looked at a fixed system size of 10×30 cm and varied the number of grid points for different cylinder radii in order to study the finite-size effects of our approach. The grid spacing Δx varied from 0.3125 to 0.078 125 cm, and by linear extrapolation we obtained the curve $\lim_{\Delta x \to 0} v_c(r)$ shown in Fig. 3. For comparison, we also give the numerically obtained solution to Eq. (7) for Reynolds numbers up to 1 drawn as thick black line. By doubling the grid size in both directions from 64×192 to 128×384 points the value of $v_c(D)$ changed by 23% for $D=0.5$ cm and by only 4.5% for $D=3$ cm. Our extrapolated value for $D=0.5$ cm lies exactly on the analytic curve, which validates our algorithm and shows that quantitative data can be obtained by this numerical method.

Whereas the finite-size error due to the grid is a purely numerical artifact, the dependence of the terminal velocity on the container geometry is well observed experimentally [3]. For spheres in three-dimensional systems an analytic expression exists for the creeping flow limit. The relevant parameter is the ratio of the sphere diameter to the tube diameter (D/L). The ratio $v_s(D/L)/v_s(0)$ is called the wall correction factor, and a first approximation, linear in D/L, is given by Eq. (6) [1,3,9]. For cylinders in two dimensions one cannot derive an analytic expression for the wall correction factor, since not even an explicit formula for $v_c^\infty := v_c(0)$ exists. We used extensive numerical studies using the implicit method outlined in Sec. III to obtain an expression for the wall correction factor for cylinders. The diameter D was varied from 0.5 to 3.5 cm, the grid spacing was set to a

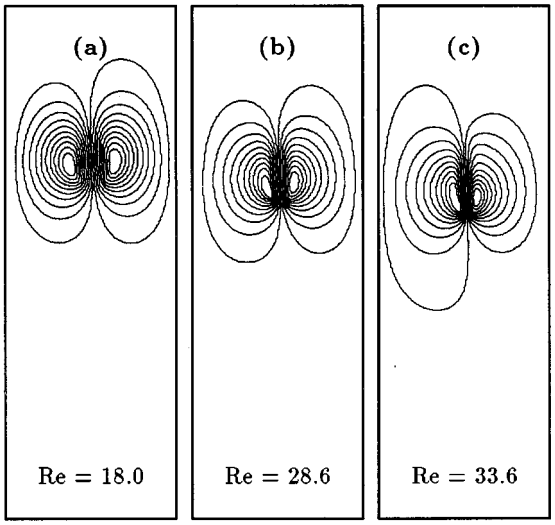

FIG. 4. Streamlines for box sizes of 10×20 cm (a), 20×60 cm (b), and 30×90 cm (c), and a particle diameter of 2 cm.

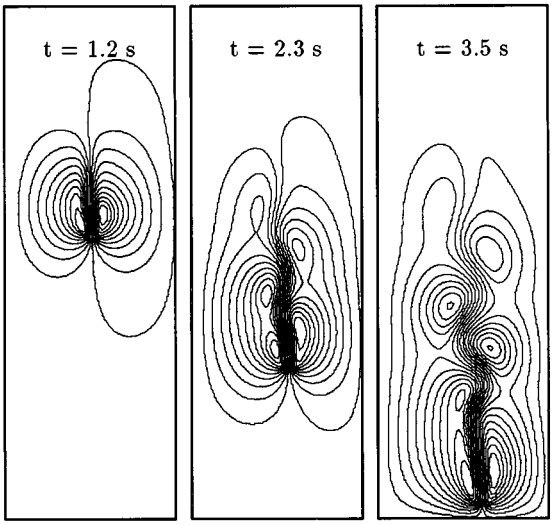

FIG. 5. Streamlines for a particle with diameter of 2.8 cm in a box of 30×90 cm at different times after particle release.

constant value of $\Delta x = 0.156\,25$ cm in order to avoid finite-size effects, and the viscosity of the fluid was set to 1 g/cm s, which is 100 times the value of water (water-glycerin mixture or certain oils). Since the only parameter that enters the Navier-Stokes equations (1) is the Reynolds number one can equally well consider water and divide all lengths by 100.

All four boundaries are considered as solid container walls with a no-slip boundary condition for the fluid. In order to quantify the effect of these boundaries, we show in Fig. 4 the computed streamlines for box sizes of 10×20 cm (a), 20×60 cm (b), and 30×90 cm (c). The corresponding times after particle release are 3.6 s (a), 7.2 s (b), and 1.1 s (c), respectively, and the particle diameter is 2 cm. The particle is located in the middle between the two vortices, and the Reynolds numbers calculated from the particle's diameter and velocity are shown in the figure. The grid size was 64×192 points. Due to the backflow effect, the particle settling is strongly affected by the ratio D/L for the geometries considered (cf. Fig. 2). The two vortices have the same size for case (a), but become clearly asymmetric for case (c), which is the start of the wake oscillations found experimentally [3].

It is reported that for cylinders wake oscillations start for Re $>$ 30, and wake shedding for Re $>$ 40 [3]. To demonstrate that our algorithm is capable of resolving this change in flow pattern for the grid sizes used, we show in Fig. 5 the computed streamlines for a sinking particle with diameter of 2.8 cm in a box of 30×90 cm at different times after particle release. The particle is located between the two lowest vortices, and the grid size was again 64×192 points. The terminal velocity was -20.5 cm/s, which was reached after 1.5 s and gives Re = 57.4. The wake oscillations which lead to wake shedding in this case are clearly visible in the third picture when the particle has nearly reached the bottom wall. Similar pictures can be found in Ref. [5] for the settling of circular and elliptical particles.

In Fig. 6, we show the values of the terminal velocity for cylinders with different diameters as function of the ratio D/L. The top curve is for $D = 0.5$ cm, and D was varied in steps of 0.5 cm to give $D = 3.5$ cm for the lowest curve. The

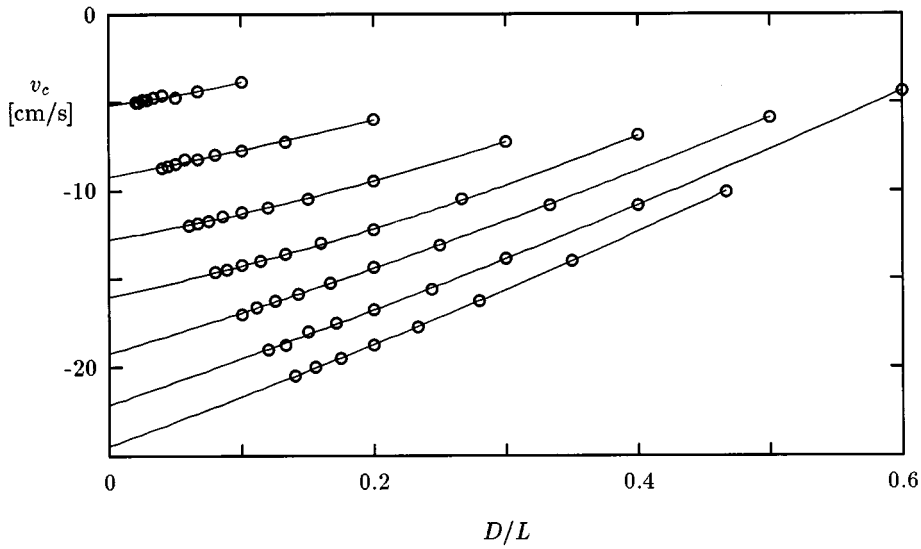

FIG. 6. Terminal velocity as function of the ratio D/L. Each curve corresponds to a different cylinder diameter with $D = 0.5$, 1, 1.5, 2, 2.5, 3, and 3.5 cm (top to bottom).

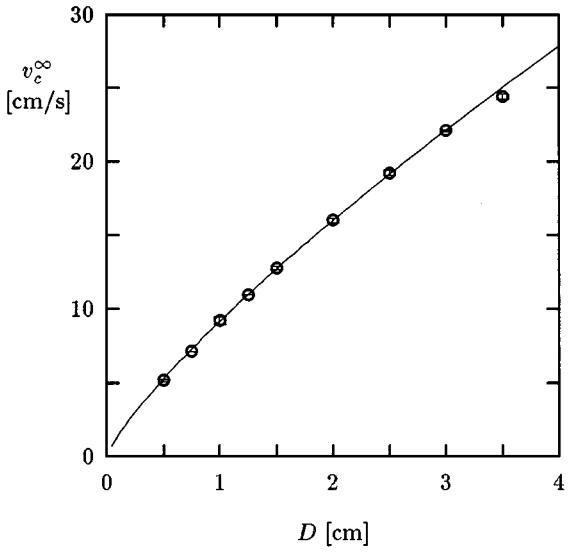

FIG. 7. Extrapolated terminal velocity for the limit $D/L \to 0$ as a function of cylinder diameter.

solid lines are quadratic least square fits for data points belonging to each value of D. It is remarkable that all data points lie on the corresponding curve.

By extrapolating each curve to $D/L \to 0$, we obtain the value of the terminal velocity $v_c^\infty(D)$ for an infinite system. These are plotted in Fig. 7, where the error bars are less than the symbol size. This can be directly compared with Fig. 3. Please note that the curve for $D/L \to 0$ starts off too high at $D=0.5$ cm compared to the numerically solved implicit equation (7), since finite-size effects could not be taken into account due to computer limitations. Nevertheless, by using the results presented in Ref. [7], one can estimate that the value for $v_c^\infty(0.5)$ will reduce by 50% but only by 10% for $v_c^\infty(3.5)$. This will bring the solution of the analytic result and the numerical simulation in perfect agreement again. Figure 7 also shows that the terminal velocity does not have a simple scaling relation with the cylinder radius, and a good

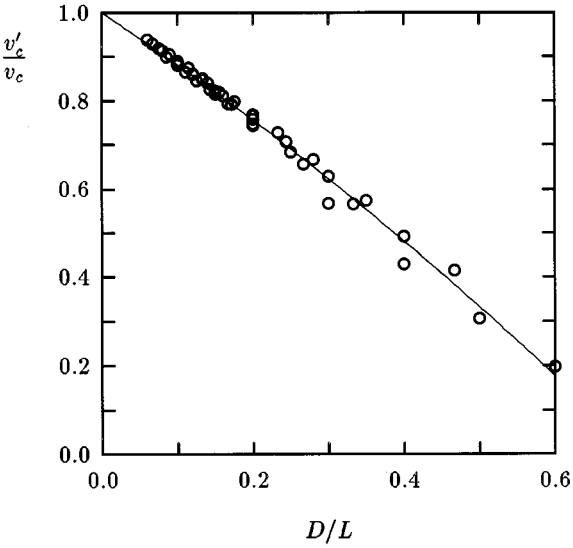

FIG. 8. Rescaled terminal velocities as a function of D/L. The solid line is the best quadratic fit to the data points.

TABLE I. Coefficients a_1 and a_2 for the quadratic approximation $f(D/L)$ for different cylinder diameters D.

D	0.5	0.75	1.0	1.25	1.5	2.0	2.5	3.0	3.5
a_1	1.86	0.99	1.53	0.98	0.99	0.97	1.16	1.14	1.10
a_2	6.34	5.23	1.07	2.21	1.51	1.13	0.46	0.33	0.34

fit was obtained by $v_c^\infty(D)=9.2\,D^{0.8}$ which is shown as a solid line. But the formula is only valid in this limited regime since towards both end points systematic deviations are already visible. Also the slope in the limit $\lim_{D\to 0} v_c^\infty$ does not agree with the analytic result, Eq. (7).

By looking at Fig. 6, one might hope that by shifting and stretching each curve all curves will fall on one universal curve. In order to test this we use as ansatz for the wall correction factor for cylinders

$$f(D/L) := \frac{v_c(D/L)}{v_c^\infty}. \tag{11}$$

This ratio is plotted in Fig. 8 for cylinder diameters ranging from 1.5 to 3.5 cm. A quadratic least square fit using all data points shown is drawn as solid line. The smaller the diameter, the more the data points systematically deviate from this *universal* curve for larger ratios D/L. For $D=0.5$ and 1.0 cm only the two leftmost points will lie on this curve. To quantify this result we write

$$f(D/L) \approx 1 - a_1 \frac{D}{L} - a_2 \left(\frac{D}{L}\right)^2, \tag{12}$$

and give the values of a_1 and a_2 in Table I for different cylinder diameters. The larger the diameter becomes, the less important the quadratic term in formula (12) becomes, which means that as a final result for the wall correction factor for cylinders we obtain

$$\frac{v_c(D/L)}{v_c^\infty} \approx \left(1 - 1.14 \frac{D}{L}\right). \tag{13}$$

V. CONCLUSIONS AND OUTLOOK

We studied the motion of cylinders under gravity (two-dimensional system) in viscous fluids and bounded geometries. The dependence of the terminal velocity of the cylinder on the diameter to box width ratio (D/L) was investigated numerically using the full Navier-Stokes equations. We obtained a first approximation of the wall correction factor as a power series in D/L and discussed its validity.

The presented algorithm, an implicit finite difference method, is easily extendable to studying real three-dimensional systems, and will be used to go beyond the creeping flow result for the wall correction factor of spheres, Eq. (6). When more time is spent to achieve a faster convergence of the numerical method, e.g., using conjugate-gradient or multigrid methods seem promising [11], it will be possible to study lubrication effects and sedimentation problems in more detail as well.

ACKNOWLEDGMENTS

We gratefully acknowledge the computer time given to us on the following parallel machines: Intel Paragon (ZAM Jülich), Cray T3D (ZIB Berlin), and IBM SP2 (HRZ Marburg). Without their use, the detailed analysis presented in this paper would not have been possible.

[1] J. Happel and H. Brenner, *Low Reynolds Number Hydrodynamics* (Martinus Nijhoff, Dordrecht, 1983).
[2] L. D. Landau and E. M. Lifshitz, *Hydrodynamik* (Akademie, Berlin, 1991).
[3] R. Clift, J. R. Grace, and M. E. Weber, *Bubbles, Drops, and Particles* (Academic, New York, 1978).
[4] B. Fornberg, J. Fluid Mech. **98**, 819 (1980).
[5] J. Feng, H. H. Hu, and D. D. Joseph, J. Fluid Mech. **261**, 95 (1994).
[6] J.-H. Chen, W. G. Pritchard, and S. J. Tavener, J. Fluid Mech. **284**, 23 (1995).
[7] G. H. Ristow, Comput. Phys. Commun. **99**, 43 (1996).
[8] D. J. Tritton, *Physical Fluid Dynamics* (Clarendon, Oxford, 1988).
[9] W. Walcher, *Praktikum der Physik* (Teubner, Stuttgart, 1974).
[10] R. H. Davis, in *Mobile Particulate Systems*, edited by E. Guazzelli and L. Oger (Kluwer, Dordrecht, 1995).
[11] R. Peyret and T. D. Taylor, *Computational Methods for Fluid Flow* (Springer, Berlin, 1983).
[12] A. J. Chorin, Math. Comput. **22**, 745 (1968).
[13] S. V. Patankar, *Numerical Heat Transfer and Fluid Flow* (Hemisphere, New York, 1980).